Co-Ni-carbon flexible composite fibres for directional magnetic actuation

Jose Garcia-Torres[a,1,*], Carol Crean[a] and Elisa Vallés[b]

[a]Department of Chemistry, University of Surrey, Guildford, GU2 7HX, Surrey, UK

[b]Grup d'Electrodeposició de capes primes i nanoestructures (Ge-CPN), Materials Science and Physical Chemistry Department and Institut de Nanociència I Nanotecnologia (IN2UB), University of Barcelona, Martí i Franques, 1, 08028, Barcelona, Spain

[1] Present Address:

Condensed Matter Physics Department, University of Barcelona, Martí i Franques, 1, 08028, Barcelona, Spain

Materials Science and Physical Chemistry Department, University of Barcelona, Martí i Franques, 1, 08028, Barcelona, Spain

Nanoscience and Nanotechnology Institute (IN2UB), University of Barcelona, Martí i Franques, 1, 08028, Barcelona, Spain

*Corresponding author: garcia.torres.jm@gmail.com

Abstract

Flexible microcomponents are being widely employed in the microelectronic industry; however; they suffer from a lack of complex movement. To address this problem, we have developed flexible, electrically conductive, magnetic composite fibres showing complex motion in three dimensions with the capacity to be selectively actuated. Flexible carbon-based fibres were prepared by wet-spinning and were subsequently modified by electrodepositing Co-Ni. The high aspect ratio of the fibre (40 µm diameter, 3.5 cm length) causes a directional dependence in the magnetostatic energy, which will allow for anisotropic actuation of the composite. Thus, the application of magnetic fields allows for a precise control of the movement with high reproducibility and accuracy.

Keywords: *carbon nanomaterials; cobalt-nickel; flexible composite fibres; wet-spinning; magnetic actuation*

1. Introduction

Since their discovery in 1991, the excellent electrical and superb mechanical properties of carbon nanotubes (CNTs) have offered enormous opportunity in the field of CNT-composite research [1]. Fabricating CNTs into macroscopic structures such as composite fibres facilitates their practical application [1]. These fibrous structures are flexible and lightweight and can be tuned to have excellent mechanical and/or electrical properties to be used as fibre-based flexible electrodes [2]. Recent progress in fibre-based composites has reported the enhanced properties of multicomponent composite fibres. For example, the introduction of other nanostructured carbons (ordered mesoporous carbons, graphene) or transition metals oxides into CNT fibres combines the advantages of the different materials resulting in high performance devices such as sensors, batteries or supercapacitors for wearable electronics [3-6].

Complex, tuneable mechanical actuation in response to environmental stimuli is essential for many applications. Microactuators, microelectromechanical systems (MEMS) or *in vivo* applications of artificial muscles are just some examples of where the actuation of composite materials can be used in soft robotics [7]. The different fields that are compatible with actuation include optical [8], electric [9], acoustic [10], gravitational [11] and magnetic [12]. The application of CNT fibres as electromechanical actuators was pioneered by Spinks and co-workers [13]. These fibres converted electrical energy into mechanical energy and exhibited torsional rotation due to a hydrostatic actuation mechanism. Peng *et al.* demonstrated that electromechanical actuation could be achieved by CNT fibres not just in electrolytes, but also in air, water and organic solvents [14]. Adding azobenzene-containing liquid-crystalline polymers to CNT composite fibres generated materials with photomechanical actuation. Upon application of UV light, rapid and reversible deformation could be achieved which is interesting for applications such as artificial muscles [15]. Other stimuli-responsive CNT composite fibres have been reported that undergo mechanical actuation in the presence of solvents [16] or water/moisture [17]. These fibres exhibited anisotropic bending/unbending or large and rapid contraction and rotation of the fibre, which are solvent and moisture driven respectively.

Particularly interesting is the wireless manipulation of magnetic actuators, which have been prepared by incorporating magnetically responsive nanostructures (e.g. nanosheets,

nanowires or nanoparticles) into polymeric materials [18,19]. These flexible magnetic composite materials have been mainly developed with thin film, multilayer or 3D geometric structures [20-22]. However, the isotropic and homogenous distribution of the magnetic particles within the polymeric matrix can make it difficult to achieve orientation control with these composites. For these reasons, different strategies have been followed to impart directional actuation such as patterning [23] or one-dimensional particle assembly [24]. Such magnetically-patterned composite actuators are able to undergo motions like bending or curling. However, most of these actuation schemes lack complex motion, effective addressability and precise shape control [25,26].

Thus, the objective of this work was the preparation of flexible magnetic composite fibres showing complex motion and precise control for applications in microactuator components. In this study, fibres were prepared by wet-spinning using nanosized carbon materials (carbon nanotubes, carbon black) and chitosan. Their electrical, mechanical and electrochemical properties were analysed. Subsequently, a magnetic Co-Ni alloy was incorporated into the fibre by electrodeposition. The morphology and the magnetic properties of the composite fibres were investigated before and after the incorporation of the Co-Ni alloy. Actuation of the magnetic composite fibres was performed by applying oscillating and continuous magnetic fields in either one, two or three directions in order to induce movements that are only possible with flexible components. The benefits of our strategy, based on the combination of the different materials, the fibre geometry and the fabrication techniques, are: (i) the incorporation of nanostructured carbons which will confer electrical conductivity to the fibre, (ii) chitosan is a suitable matrix material for magnetic composites due to its biocompatibility and low cost [27], (iii) the soft-magnetic character of the Co-Ni system enabling the fibre to be wirelessly controlled under low magnetic fields, and corrosion resistance allowing the fibre to be used in aggressive fluids [28], (iv) the fibres are micron-sized in diameter which is of interest for microcomponents in MEMS, (v) the fibre shape facilitates shape magnetic anisotropy and will allow selective actuation in 3D depending on the applied magnetic field, (vi) wet-spinning is a convenient approach to developing multifunctional fibres in a continuous and scalable way [29] and (vii) electrodeposition is an easy technique to electrodeposit magnetic materials with high

speed, mild conditions (e.g. room temperature, atmospheric pressure,…) and good reproducibility [30].

2. Materials and Methods

Materials

Carbon black (CB) and multiwall carbon nanotubes (CNT) were purchased from Timcal Graphite & Carbon and Nanocyl respectively. Details of the carbon nanomaterials are summarised in Table 1. More detailed properties and characteristics can be found in the suppliers' technical data sheets and/or other published papers [31-34]. Chitosan powder, acetic acid (CH_3COOH) (99.8%), sodium dodecyl benzene sulfonate (SDBS), cobalt chloride (II) ($CoCl_2$), nickel chloride (II) ($NiCl_2$), boric acid (H_3BO_3) and hydrochloric acid were obtained from Sigma Aldrich.

Table 1. Summary of the CNT and carbon black characteristics supplied by the manufacturers.

Carbon nanomaterial	Product name	Diameter (nm)	Length (mm)	Structure
Carbo nanotube	Nanocyl^{TM} NC7000	9.5	1.5	Amorphous
Carbon black	Super P Carbon black	30-40	---	Amorphous

Methods

Flexible magnetic composite fibres were prepared by a two-step process as illustrated in Figure 1. First, carbon-based fibres were prepared by wet-spinning using two different dispersions: (i) 100% CNTs and (ii) 90% CNT and 10% CB. Carbon nanomaterials (dispersion (i): 0.1 wt.% CNT, dispersion (ii) 0.09 wt.% CNT and 0.01 wt.% CB) were dispersed in water using sodium dodecyl benzene sulphonate (SDBS) (0.15 wt.%) as dispersant. A horn sonicator (amplitude: 30 %, power: 500 W and frequency: 20 kHz) was employed to break the aggregates and facilitate the dispersion of the carbon nanomaterials. During sonication,

the dispersion was immersed in a water/ice bath in order to avoid overheating. After that, the dispersion was extruded out of a spinneret at 10 ml/min into the coagulation bath -0.25 wt.% chitosan and 0.5 wt.% CH_3COOH- where the coagulation and fibre formation took place. The coagulation bath was rotated at 50 rpm. Fibres could be made in lengths of up to a meter at a time. Finally, fibres were extracted, washed and dried under tension.

In a second step, Co-Ni electrodeposition onto the dried fibres was carried out employing the following electrolyte: 0.2 M $CoCl_2$, 0.9 M $NiCl_2$ and 0.5 M H_3BO_3. The pH was adjusted in the range 1-3 with HCl. Solutions were de-aerated by argon bubbling before and during the experiment. Electrochemical experiments were carried out in a conventional three-electrode cell. The carbon-based fibres were used as the working electrode while the reference and the counter electrodes were Ag/AgCl/1 M NaCl and a platinum spiral, respectively. Voltammetric experiments were carried out at quiescent conditions at a scan rate of 100 mV s^{-1}. Co-Ni electrodeposition was performed by chronoamperometry.

Scanning electron microscopy (SEM) was employed to characterize the morphology of the fibres before and after electrodeposition using a Hitachi H-4100FE and a JSM 7100 microscope. Energy dispersive spectroscopy (EDS) was performed to qualitatively determine the elemental composition. Raman microscopy was carried out using a Renishaw inVia spectrometer with a 532 nm laser. Electrical conductivity was evaluated by the four-probe method, where a constant current was applied and the resultant voltage measured by a Keithley 2001 multimeter. Magnetic measurements were taken in a SQUID magnetometer at 300 K in a helium atmosphere. The magnetisation-magnetic field curves were recorded maintaining the samples parallel and perpendicular to the applied magnetic field. Magnetic actuation of the fibres (40 μm diameter, 3.5 cm length) was carried out in a home-made system consisting of custom-made coils oriented along three perpendicular directions. Quantitative results for actuation were obtained in a Helmholtz configuration. Each coil was made by ∼1100 turns with 4 mm diameter wire and had 5 and 2 cm of outer and inner diameter, respectively. The magnetic field was achieved by connecting the coils to a waveform generator (TTi TGA1244) commanded by a current amplifier (IMG STA-800) to generate the oscillating field or to a DC power to obtain a constant magnetic field. Different frequencies (1 and 5 Hz) and magnetic field strengths (1-5 mT) were applied to study their influence on the fibres motion. Three different fibres were actuated to study reproducibility.

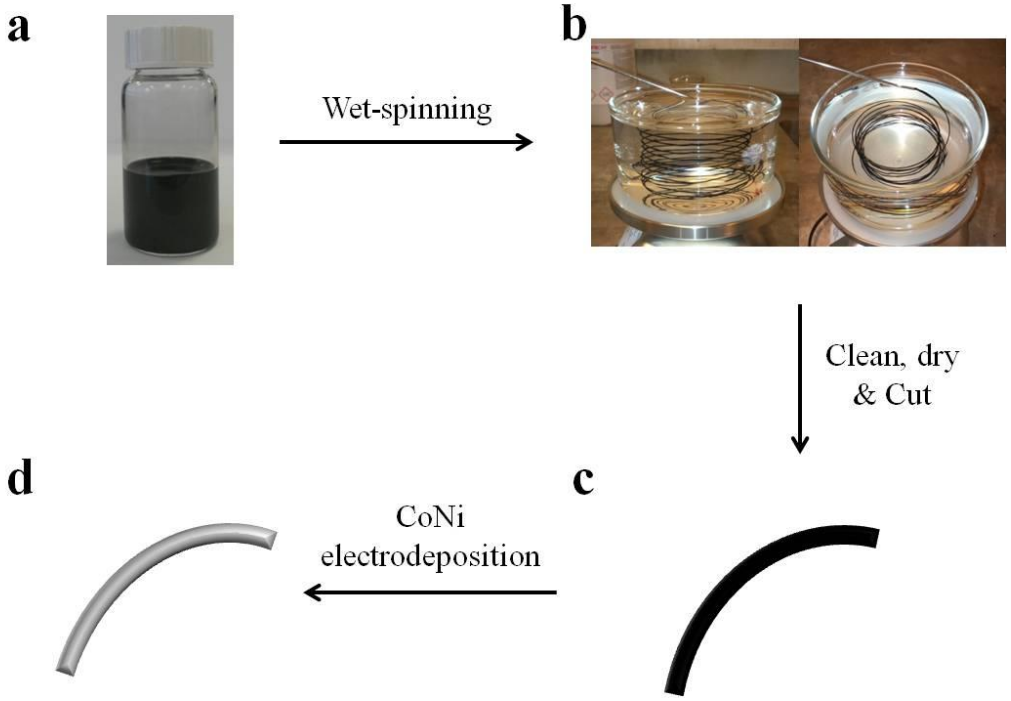

Figure 1. Scheme showing the experimental procedure to obtain the magnetic flexible fibres: a) image of a homogenous dispersion of carbon black and carbon nanotubes, b) wet-spinning of the dispersion into the coagulation bath, c) cleaning with water, dried under an applied stress and cut into shorter fibres and d) electrodeposition of Co-Ni alloy in the fibre.

3. Results and Discussion

Flexible Co-Ni-CNT-CB composite fibres were prepared by a two-step process. First, carbon-based flexible fibres were prepared by wet-spinning. Two different dispersions were spun into a chitosan polymer coagulation bath i) 100 % CNTs and ii) 10 % carbon black and 90 % CNTs. The synergistic effect of combining carbon nanotubes and carbon black has been previously shown [35]. Both of these fibres were conductive with electrical conductivities of 10 and 15 S/cm respectively. The mechanical properties of the fibres, made from dispersions with 10 % carbon black and 90 % CNTs, were superior to fibres spun from dispersions containing 100% CNTs as can be seen in Figure 2a. Tensile strengths of 22.9 and 13.8 MPa and breaking strain values of 1.5 and 2.8 % were measured for the CB-CNT and CNT fibres respectively. The higher tensile strength and higher strain values of the CB-CNT fibres indicates their capacity to withstand bigger loads and experience higher elongations before breaking. Moreover, the Young modulus (*E*) calculated from the linear part of the

stress-strain curve shows that carbon black-CNT based fibres had superior stiffness (E = 18.8 MPa) than CNT fibres (E = 11.4 MPa). This means that CB-CNT fibres have higher rigidity and therefore lower elastic deformation. Overall however, the stiffness of these fibres is very low meaning they are deformable and therefore flexible; the E values measured are of the same order of magnitude as polymer based composites such as low-density polyethylene (LDPE) and some rubber-based composites [21]. There was also an improvement in the electrochemical properties of the CB-CNT fibre -higher current, more square shape- compared to fibres spun from dispersions containing 100% CNTs (Figure 2b). For these reasons, the fibre made from the 10 % carbon black and 90 % CNT dispersion was taken forward for electrodeposition of the magnetic alloy. After cleaning and drying longer fibres under stress, they were shortened and employed as electrodes for the electrodeposition of the Co-Ni alloy. This latter step was carried out to confer magnetic properties to the fibres. Devices containing Co-Ni have been successfully used for magnetic actuators [36] or magnetic micromechanical structures [37]. The Co-Ni system was selected because Co increases the magnetisation of saturation of the system while nickel improves the stability and corrosion resistance of the material [27]. In order to select a suitable electrodeposition potential, an electrochemical study was performed. Cyclic voltammetry was carried out in order to study the potential range at which both metals can be simultaneously electrodeposited. The electrolyte composition was selected considering not only the standard potential of Co ($E°$ = -0.499 V) and Ni ($E°$ = -0.470 V) but also the anomalous co-deposition of the Co-Ni system, where the less noble metal (Co) is electrodeposited more easily [39]. Therefore, the concentration of the Co salt in the electrolyte (0.2 M) was lower than that of the Ni precursor (0.9 M).

Figure 2c shows the cyclic voltammetry recorded from the selected electrolyte containing the Co(II) and Ni(II) salts. A clear reduction current was observed from potentials at approximately -0.7 V (*vs.* Ag/AgCl) and the continuous current that increased during the cathodic scan corresponds to the simultaneous reduction of Co(II) and Ni(II). The closeness in their reduction potentials prohibits the observation of a separate reduction for each ion. The high concentration of the cationic metals in the electrolyte and the electrocatalytic properties of the deposited metals with respect to hydrogen evolution explain the non-observance of a clear reduction peak. During the positive, anodic scan, a single oxidation

peak was recorded. This unique peak is attributed to the oxidation of a Co-Ni solid solution formed during the cathodic scan. This result is in agreement with previous reports [27] and the Co-Ni phase diagram, where total miscibility between the two metals is observed [39].

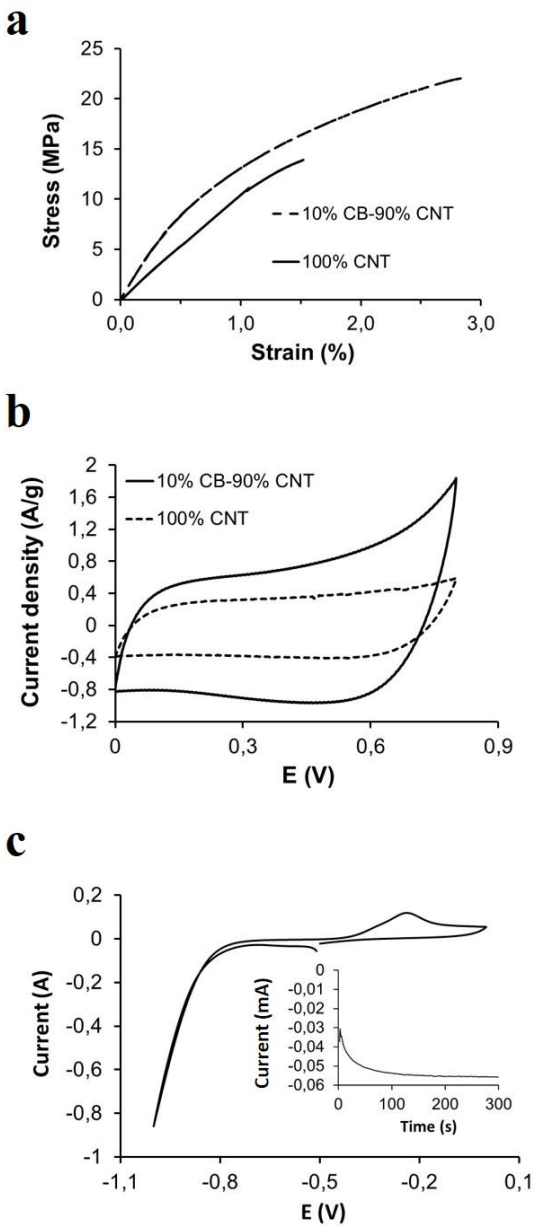

Figure 2. (a) Mechanical properties of the fibres containing CNTs only and carbon black mixed with CNTs. (b) Cyclic voltammetry *vs.* Ag/AgCl at 100 mV s^{-1} of fibres containing CNTs only and carbon black mixed with CNTs. (c) Electrochemical characterisation of the electrolyte employed for Co-Ni deposition: Cyclic voltammetry *vs.* Ag/AgCl at 100 mV s^{-1} of the Co-Ni solution with one fibre, and (inset) chronoamperometric curve of Co-Ni deposition by applying -1100 mV for 300 s.

The deposition of Co-Ni onto the fibres was carried out potentiostatically, with an applied potential of -1100 mV in order to favour a high deposition rate of the alloy while avoiding hydrogen evolution that could hinder metal incorporation into the fibres. The inset in Figure 2c shows a representative chronoamperometric curve corresponding to a potentiostatic Co-Ni deposition on the carbon-based fibre. The shape of the curve is typical of a nucleation and growth deposition process followed by a stabilisation in the current when the deposition attains a steady-state regime. After electrodeposition, the Co-Ni alloy content represents 35% of the total fibre weight.

Scanning electron microscopy was used to characterise the composite fibres before and after their modification with the Co-Ni alloy. Carbon-based fibres showed diameters in the range of 40-50 µm with a corrugated surface structure aligned along the fibre axis (Figure 3a). The fibre cross-section allows the observation of CNTs and carbon black nanoparticles in the fibre core while the chitosan polymer forms a shell around them (Figure 3b). After Co-Ni deposition no noticeable differences in the fibre surface morphology was detected (Figure 3c). The same corrugated surface was observed without any appreciable Co-Ni deposit formed onto the fibre. However, a very different morphology can be seen at the fibre cross-section (Figure 3d) where a globular surface morphology can be seen at the higher magnified SEM image. The Co-Ni alloy that deposited in the fibre core appears uniform and compact (Figure 3d). In order to unequivocally assign the change in the morphology to the Co-Ni electrodeposition, backscattered electrons were collected and energy dispersive spectroscopy (EDS) was carried out. Figure 3e shows the backscattered electron image where two different regions can be observed: a dark and a bright region. While the brighter area corresponds to heavy elements (e.g. metals); the darker areas are due to lighter elements such as carbon or polymer substances. From this backscattered image, a homogeneous distribution of the Co-Ni alloy can be observed in the fibre core. The EDS spectrum of the fibre core confirms the presence of Co-Ni (Figure 3f) and suggests that the composition of the magnetic deposit is 60 wt.% Co and 40 wt.% Ni. The signal from the C element is also present, as expected. Peaks were also observed in the EDS spectrum between 1-3 eV which correspond to impurities from the electrolyte (e.g. chloride ions) and/or the dispersant (SDBS) used during the dispersion of the carbon nanomaterials (e.g.

sulphur). The electrodeposition of Co-Ni inside the fibre can be explained by the fact that the fibre swells when immersed in water, due to the hydrophilic nature of the chitosan polymer. Fibre swelling favours the introduction of the electrolyte into the fibre where the conductive carbon nanomaterials are present, facilitating alloy deposition within the fibre core. Finally, it should be noted that no discernible increase in the fibre diameter was observed and no cracks were detected on the fibre surface, suggesting that the Co-Ni alloy did not initiate internal stress.

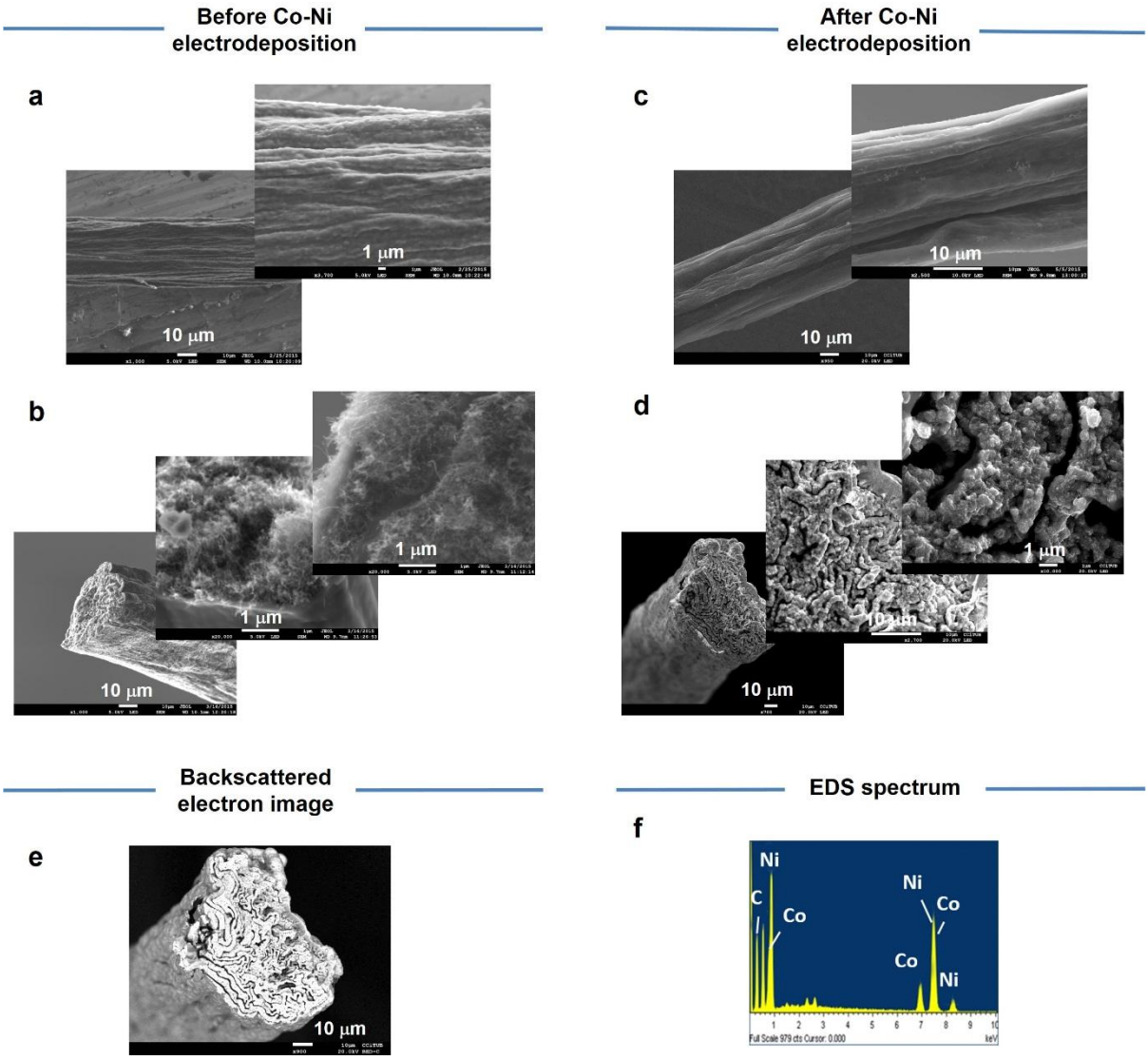

Figure 3. (a) SEM images of the surface of carbon-based fibres. (b) SEM images of the cross-section of carbon-based fibres. (c,d) SEM images of the surface and cross-section of Co-Ni-modified carbon-based fibres. (e) backscattered electron image. (f) EDS spectrum of the Co-

Ni modified fibre cross-section. Non-labelled small peaks in the spectrum correspond to impurities from the electrolyte (e.g. chloride ions) and/or the dispersant (e.g. sulphur).

Raman spectroscopy of the fibres is shown in Figure 4. Figure 4a shows the Raman spectrum of the bare carbon-chitosan fibre, which had not been immersed in the electrolyte containing the magnetic precursor salts. The D and G bands associated with the disorder (D-band) and the tangential mode vibrations (G-band) of the sp^2 carbons in the carbon nanomaterials were measured at 1348 cm^{-1} and 1590 cm^{-1} respectively [40]. The Raman spectrum of the fibre containing Co-Ni also shows peaks corresponding to the D and G bands of carbon. In addition, peaks were observed during Raman measurements attributable to the presence of Co and Ni mixed oxides. These peaks are expected since Co-Ni alloy is easily oxidised in air leading to the formation of surface oxides. Windisch *et al.* have published extensively on the composition of cobalt–nickel oxide films analysed by Raman spectroscopy [41]. They assert that the predominant component of these oxides is typically a spinel structure, $NiCo_2O_4$, in which the lattice parameters shift depending on the substitution of Co for Ni in the spinel structure. Vibrations of Co_3O_4 associated with octahedral Co^{3+} have been observed at 693 cm^{-1}. This band weakens and shifts to a lower frequency, as the Co^{3+} is replaced by Ni^{2+} in $NiCo_2O_4$, and is observed in Figure 4b at 649 cm^{-1} and 661 cm^{-1}, depending on where on the fibre the spectrum was taken from. Peaks due to cubic NiO can also be seen at 510 cm^{-1}, which shifted to a higher frequency of 540 cm^{-1} in Figure 4b, which has been attributed to substitution of Co for Ni in the spinel structure. These results suggest that the Co-Ni modification of the fibre yields a mixture of deposits with different stoichiometry and structure as previously reported which have a surface oxide layer [42].

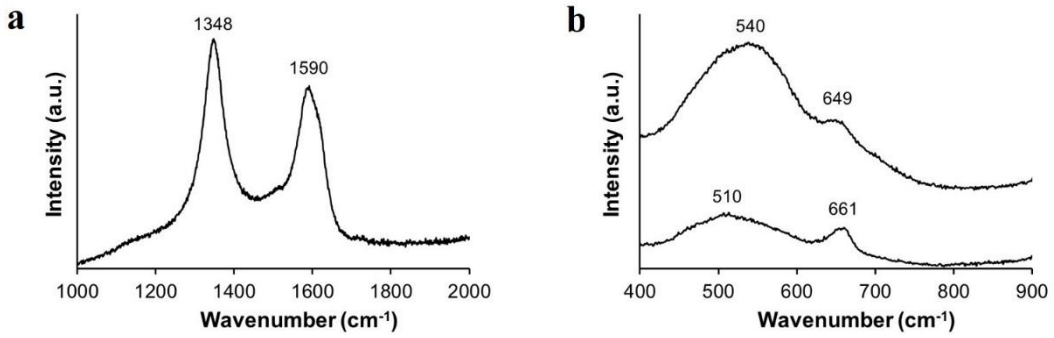

Figure 4. (a) Raman spectra of the bare carbon black-CNT fibre. (b) Raman spectra of the Co-Ni coated fibre.

Magnetic measurements were carried out in order to evaluate the anisotropic magnetic properties of these flexible Co-Ni-carbon composite fibres. Magnetisation-magnetic field curves were recorded with the applied magnetic field either parallel or perpendicular to the fibre axis, and represented in both *M-H* and M/M_s-*H* form (Fig. 5a). The magnetization of saturation (M_s) of the material, were g refers to the amount of the magnetic material contained in the fibre, agrees with the expected value for a Co-Ni alloy [43], showing an intermediate value between the M_s of Co (143 emu g^{-1}) [44] and Ni (55 emu g^{-1}) [45]. The magnetic curves show a clear ferromagnetic behaviour with low coercive values, of approximately 10 mT (in parallel) and 18 mT (in perpendicular configuration). These low values suggest the soft magnetic character of the composite fibres. This makes it interesting because low magnetic fields (a few mT) are enough to get the fibres actuated. From the *M-H* curves we can observe that the easy axis of magnetization is parallel to the fibre axis. Shape anisotropy is the prevailing type of magnetic anisotropy in this system, due to the shape and dimensions of the fibres (micron-sized diameter with lengths in centimetres). Despite the presence of surface oxides on the fibre as confirmed by Raman spectroscopy, the magnetic character of the Co-Ni composite fibre facilitates magnetic actuation, while the shape of the fibre enables a different response when the magnetic field is applied in different directions.

Actuation experiments were conducted on the Co-Ni-carbon composite fibres (40 μm in diameter and 3.5 cm in length) suspended within coils oriented along three perpendicular directions –x, y and z–. The oscillating magnetic fields were modified in terms of frequency and field strength and were applied in either one, two or three directions. This was done to create a magnetic field in three directions simultaneously and use them to demonstrate the 3D multi-actuation of the composite fibres.

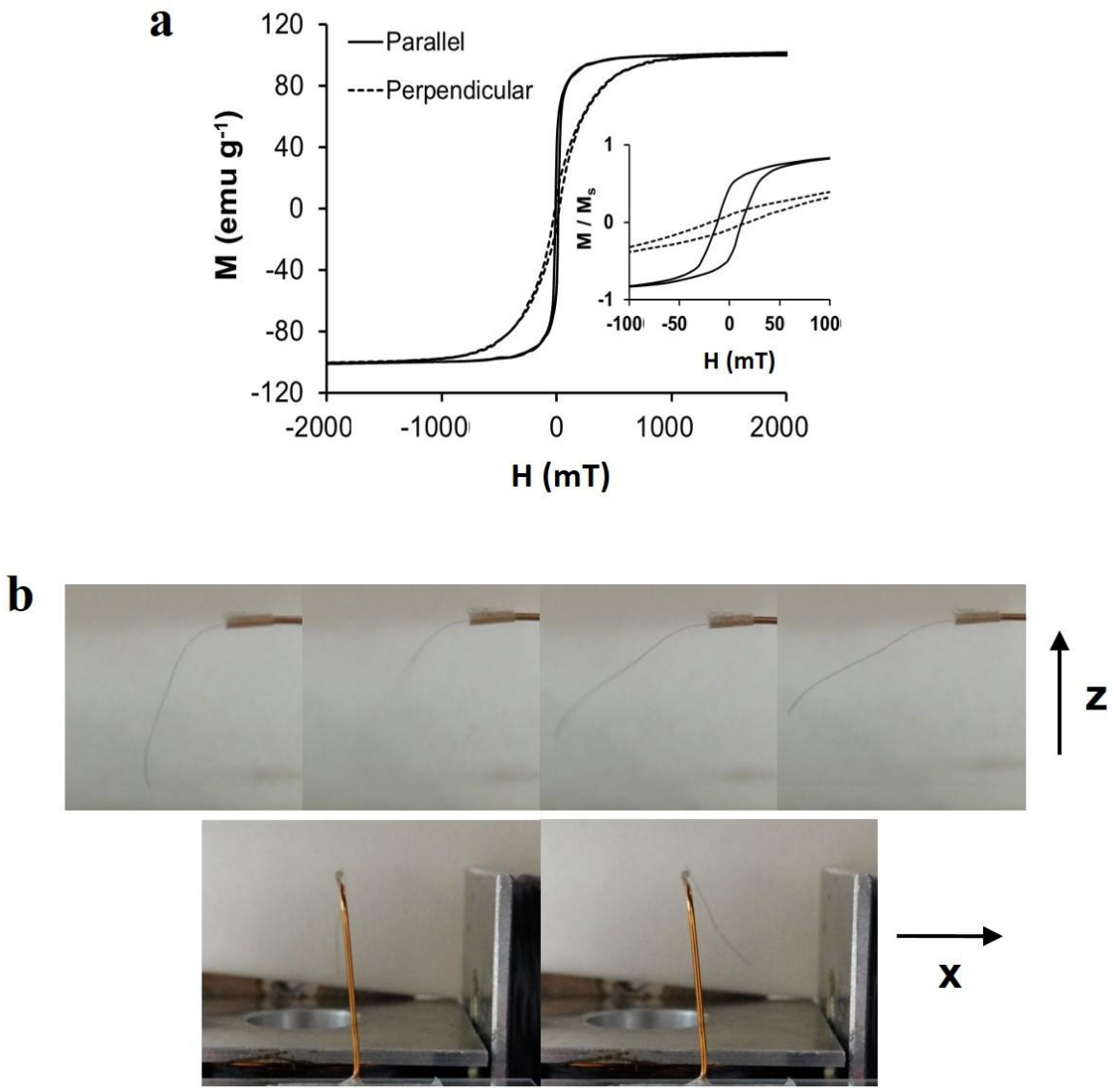

Figure 5. (a) Normalized magnetization-magnetic field curves of Co-Ni carbon-based fibres parallel and perpendicular to fibre axis. (b) Photographs of the fibre when the magnetic field is applied in either z or x directions.

First, a unidirectional magnetic field was applied to the fibres in either the x, y or z direction. The fibres responded to all fields, acting as a pendulum and trying to align to them. Figure 5b shows two image sequences where the fibre underwent actuation when the magnetic field was applied either in the z or x directions. Figures 6a and b show how the position of the fibre varied as a function of time for different frequencies and intensities of the applied field (see also videos S1, S2 and S3, supporting information). A sinusoidal plot for the

position was observed because of the sinusoidal nature of the applied magnetic field. Fibre height increased from approximately 1.8 cm to approximately 3.2 cm when the magnetic field strength was increased from 2 to 5 mT. A small difference in the fibre height between the two frequencies (1, 5 Hz) can also be observed which is attributed to the magnetic field frequency dependence. In the low frequency range (1-15 Hz) the higher the frequency, the higher the magnetic field strength, and hence the higher the height. An influence of the applied frequency was also observed. When the frequency of the magnetic field was increased from 1Hz to 5Hz, the fibre moved faster as the number of oscillations per unit of time was higher. For example, at a ω=1Hz, the fibre completes 1 cycle of the oscillating magnetic field, while at a ω=5Hz, the fibre is able to make 5 cycles in the same time. These results demonstrate that the fibre's height, and therefore the motion, can precisely be controlled by modifying the magnetic field parameters (frequency and strength). Excellent accuracy was observed during the actuation as the same height profile was obtained even after 2000 cycles. Calculated standard deviations from the actuation profiles (see data in Fig. 6a,b) are of the order of a few hundredths of centimetres – representing a change not higher than 2% – which clearly prove that the actuation is very reproducible. The reproducibility of actuation heights after thousands of cycles indicates minor change in the materials during the experiments which is essential for a long cycle life. Similar qualitative results have been achieved with longer or shorter fibres, with a different actuation height achieved by the fibres, depending on the fibre length.

To better analyse the height-magnetic field dependence, the fibre height was monitored against the magnetic field strength applied with coils in a Helmholtz configuration. Figure 6c shows the deflection of the fibre from the equilibrium position as a function of the applied magnetic field. To compare the symmetry of the pendular motion, the fibre deflection in both sides of the motion (near the two coils) is represented. As it can be observed, the higher the magnetic field applied, the higher the height achieved by the fibre. On the other hand, a symmetric motion is recorded as fibres reach almost the same height at the same magnetic field strength. High reproducibility in the measurements was checked. These results demonstrate that the fibre's height, and therefore the motion, can be controlled by modifying the magnetic field parameters (frequency and strength).

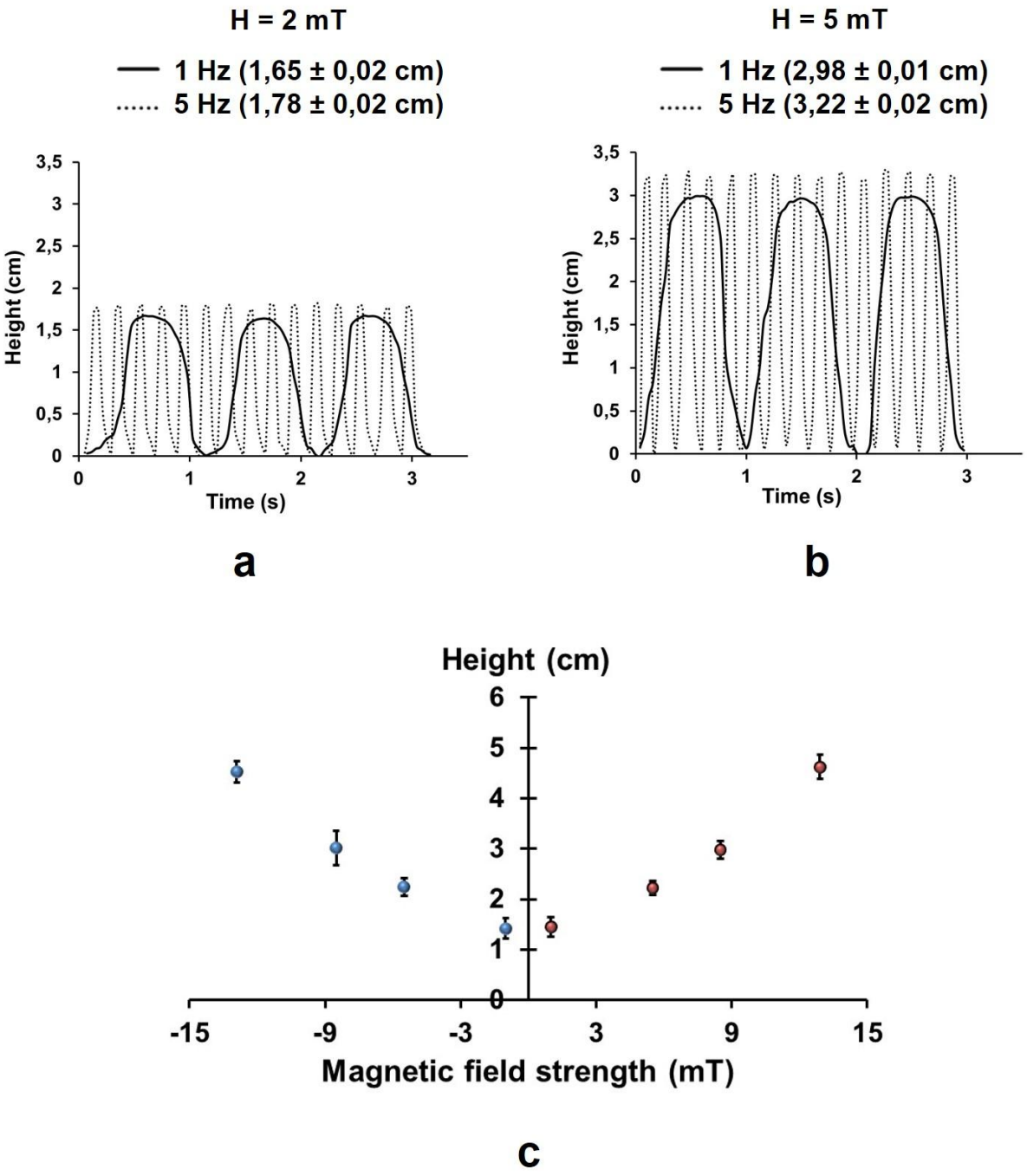

Figure 6. 1D actuation of the fibre using linearly oscillating magnetic fields. Change in the tip position of the fibre when the magnetic field was (a) 2 mT and (b) 5 mT for two different frequencies (1Hz and 5 Hz). (c) Variation of the height achieved by the fibre with the magnetic field strength.

Fibres were also actuated in 2D rotating fields generated by simultaneously applying oscillating fields in x-y, y-z or x-z planes. Coupling two oscillating fields applied in two

perpendicular directions generated a rotating field in the corresponding plane (Figure 7a). Thus, when an x-y rotating field was applied the fibre circled in the corresponding plane as it tried to align to the generated rotating field. Again, the magnetic field frequency and intensity applied to the fibres were modified (Videos S4, S5 and S6, supporting information). While the frequency of the field has an impact on the angular velocity, the field intensity influences the diameter of the circle traversed. Thus, the higher the frequency, the higher the angular velocity, and the higher the magnetic field, the higher the diameter navigated by the fibres.

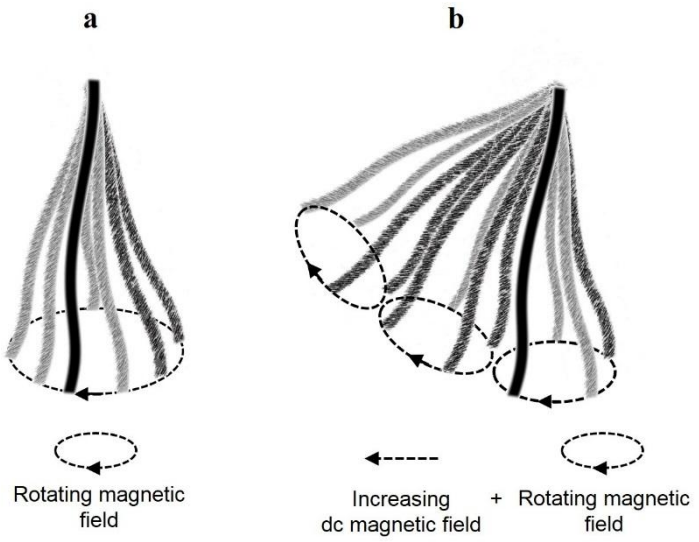

Figure 7. Cartoons representing (a) the circle described by the fibre when a rotating magnetic field is applied, (b) the circles at certain heights when an increasing dc magnetic field is simultaneously applied to the rotating field.

Fibres were also actuated by applying a rotating field in the x-y plane while simultaneously applying a continuous field in the z direction (as described in Figure 7b). This combination of fields allowed the fibres to be actuated in 3D. When the dc field applied in the z direction was constant, the fibre tracked a circle at a certain height (Videos S6, S7 and S8, supporting information). The height was dependent on the intensity of the applied field: the higher the applied dc field, the higher the height achieved by the fibre. On the other hand, if the dc z magnetic field was continuously modified, the fibre had a helical motion from the lowest to the highest point.

From these experiments, reversible and reproducible actuation of the magnetic fibres can be observed in one, two or three directions even after thousands of cycles. The different modes of motion are feasible due the cylindrical shape of the fibres and therefore the inherent magnetic anisotropy and flexibility. Recently, magnetic composites have been prepared by depositing a magnetic material on polymeric flexible membranes as PDMS or incorporated in the form of particles inside polymers during their preparation process [20-22]. Primarily, these papers report the actuation of membranes in one direction and a few for deflection and twisting. The mechanical properties of these composites are similar in terms of tensile strength to our fibres. However, one disadvantage of our fibres is the low strain values measured when compared with those composites. In summary, multifunctional fibres have been fabricated with the following advantages: they are flexible and electrically conductive, they show simple and complex motions -oscillation in one direction, rotation in a plane and helical motion in 3D- showing reproducibility even after thousands of actuating cycles and they can be easily prepared without the need for complicated techniques to facilitate magnetic patterning. These fibres may be suited for applications such as magnetically controlled components for MEMS.

4. Conclusions

In summary, we have successfully developed magnetically actuated flexible Co-Ni-carbon composite fibres in a two-step process. Fibres show triple functionality –flexibility, electrical conductivity, magnetic properties– which make them interesting for MEMS. The actuation of the fibres in a unidirectional oscillating magnetic field leads to a pendular motion of the fibre. The height achieved by the fibre can be controlled by tuning the magnetic field strength. Moreover, applying more complex fields allows the in-plane rotation or the helical motion of the fibres. The interaction of the magnetic anisotropy associated with the shape and different applied magnetic fields allows the actuation of the microscale fibres in 1D, 2D or 3D. The flexible fibres with magnetically driven and directional mechanical responses with high reproducibility even after thousands of cycles could be successfully employed for remote directional manipulation of soft actuators, valves, and motors and for other soft robotic applications at the microscale.

Acknowledgements

This research was supported by EPSRC projects 'Advanced fibre-based energy storage for wearable applications' (EP/K035002/1) and 'High Spec Raman Spectrometer Regional Facility' (EP/M022749/1) and Spanish Government grants TEC2014-51940-C2-2-R from *Ministerio de Economía y Competitividad* (MINECO), the latter co-financed by FEDER.

References

[1] W. Lu, M. Zu, J.-H. Byun, B.-S. Kim and T.-. Chou, Adv. Mater. 24 (2012) 1805–1833.

[2] C. Lynam, S. E. Moulton and G. G. Wallace, Adv. Mater. 19 (2007) 1244–1248.

[3] Z. Yang, J. ren, Z. Zhang, X. Chen, G. Guan, L. Qiu, Y. Zhang and H. Peng, Chem. Rev. 115 (2015) 5159-5223.

[4] P. Shi, L. Li, L. Hua, Q. Qian, P. Wang, J. Zhou, G. Sun and W. Huang, ACS Nano 11 (2017) 444-452.

[5] L. Hua, P. Shi, C. Yu, R. Chen, Y. Gong, Z. Du, J. Zhou, H. Zhang, X. Tang, G. Sun and W. Huang, ACS Appl. Mater. Interf. 9 (2017) 37022-37030.

[6] G. Sun, X. Zhang, R. Lin, B. Chen, L. Zheng, X. Huang, L. Huang, W. Huang, H. Zhang and P. Chen, Adv. Electronic Mater. 2 (2016) 1600102-1600106.

[7] A. Miriyev, K. Stack and H. Lipsin, Nat. Comm. 8 (2017) 596-603.

[8] D. G. Grier, Nature 424 (2003) 810-816.

[9] Y. Huang, K. L. Ewalt, M. Tirado, R. Haigis, A. Forster, D. Ackley, M. J. Heller, J. P. O'Connel and M. Krihak, Anal. Chem. 73 (2001) 1549-1559.

[10] A. Nilsson, F. Petersson, H. Jonsson and T. Laurell, Lab Chip 4 (2004) 131-135.

[11] C. P. Royall, C. M. V. Esther, B. Alfons van and T. Hajime, J. Phys.: Condens. Matter 20 (2008) 404225-404232.

[12] R. M. Erb, J. J. Martin, R. Soheilian, C. Pan and J. R. Barber, Adv. Mater. 26 (2016) 3859–3880.

[13] J. Foroughi, G. M. Spinks, G. G. Wallace, J. Oh, M. E. Kozlov, S. Fang, T. Mirfakhrai, J. D. W. Madden, M. K. Shin, S. J. Kim and R. H. Baughman, Science 334 (2011) 494-497.

[14] W. Guo, C. Liu, F. Zhao, X. Sun, Z. Yang, T. Chen, X. Chen, L. Qiu, X. Hu and H. Peng, Adv. Mater. 24 (2012) 5379–5384.

[15] X. Sun, W. Wang, L. Qiu, W. Guo, Y. Yu and H. Peng, Angew. Chem. Int. Ed. 51 (2012) 8520 –8524.

[16] X. Lu, Z. Zhang, H. Li, X. Sun and H. Peng, J. Mater. Chem. A 2 (2014) 17272–17280.

[17] S. He, P, Chen, L, Qiu, B. Wang, X. Sun, Y. Xu and H. Peng, Angew. Chem. Int. Ed. 54 (2015) 14880 –14884.

[18] F. Hua, T. Cui and Y.M. Lvov, Nano Lett. 4 (2004) 823-825.

[19] M. Molina, M. Asadian-Birjand, J. Balach, J. Bergueiro, E. Miceli and M. Calderón, Chem. Soc. Rev. 44 (2015) 6161-6186.

[20] M. M. Said, J. Yunas, R.E. Pawinanto, B.Y. Majlis and B. Bais, Sens. Actuat. A 245 (2016) 85–96.

[21] B.A.Evans, B.L. Fiser, W.J. Prins, D.J. Rapp, A.R. Shields, D.R. Glass and R. Superfine, J. Magnet. Magnet. Mater. 324 (2012) 501–507.

[22] D.C. Stanier, J. Ciambella and S.S. Rahatekar, Composites: Part A 91 (2016) 168–176.

[23] J. Kim, S.E. Chung, S.-E. Choi, H. Lee, J. Kim and S. Kwon, Nat. Mater. 10 (2011) 747-752.

[24] S.R. Mishra, M.D. Dickey, O.D. Velev and J.B. Tracy, Nanoscale 8 (2016) 1309-1313.

[25] S.A. Wilson *et al.,* Mater. Sci. Eng. 56 (2007) 1-129.

[26] K.I. Winey and R.A. Vaia, MRS Bull. 32 (2007) 314-319.

[27] D.H.K. Reddy and S.-M. Lee, Adv. Coll. Interf. Sci. 201-202 (2013) 68-93.

[28] J. Garcia-Torres, C. Gispert, E. Gomez and E. Valles, Phys. Chem. Chem. Phys. 7 (2015) 1630-1636.

[29] R. Jalili, S.H. Aboutalebi, D. Esrafilzadeh, K. Konstantinov, J.M. Razal, S.E. Moulton and G.G. Wallace, Mater. Horiz. 1 (2014) 87-91.

[30] J. Garcia-Torres, E. Valles and E. Gomez, J. Phys. Chem. C 114(19) (2010) 9146-9152.

[31] S.A. Nanocyl, NANOCYL™ NC7000 series – Product Datasheet – Thin Multi-Wall Carbon Nanotubes (12th July 2016 – V08) (http://www.nanocyl.com/wp-content/uploads/2016/07/DM-TI-02-TDS-NC7000-V08.pdf) (last accessed: 21st November 2017)

[32] R.M. Gnanamuthu and C.W. Lee, Mater. Chem. Phys. 130 (2011) 831-834

[33] V. Palomares, A. Goñi, I. Gil de Muro, I. de Meatza, M. Bengoechea, I. Cantero and T. Rojo, J. Power. Sources 195 (2010) 7661-7668

[34] C.M. White, R. Banks, I. Hamerton and J.F. Watts, Progr. Org. Coat. 90 (2016) 44-53

[35] J. Garcia-Torres and C. Crean, Adv. Sustain. Syst. (2017). Accepted. DOI: 10.1002/00143.

[36] J. Casals-Terré, M. Duch, J.A. Plaza, J. Esteve, R. Pérez-Castillejos, E. Vallés and E. Gómez, Sens. Act. A 162 (2010) 107-115.

[37] P. Cojocaru, L. Magagnin, E. Gómez, E. Vallés, F. Liu, C. Carraro and R. Maboudian, J. Micromech. Microeng. 20 (2010) 125017-125022.

[38] E. Gómez, J. Ramirez, E. Vallés, J. Appl. Electrochem. 28 (1998) 71-79.

[39] H. Baker, Introduction to phase diagrams, alloy phase diagrams. ASM Handbook, ASM International, Cleveland, 1992. pp.94.

[40] M.S. Dresselhaus, G. Dresselhaus, R. Saito and A. Jorio, Phys. Rep. 409 (2005) 47–99.

[41] C. F. Windisch Jr., K. F. Ferris and G. J. Exarhos, J. Vac. Sci. Technol. A 19 (2001) 4, 1647-1651.

[42] J. Vilana, E. Gomez and E. Vallés, Appl. Surf. Sci. 360 (2016) 816-825

[43] M. Duch, J. Esteve, E. Gómez, R. Pérez-Castillejos and E. Vallés, J. Electrochem. Soc. 149 (2002) C201-C208.

[44] W. Gong, H. Li, Z.R. Zhao and J.C. Chen, J. Appl. Phys. 69 (1991) 5119-5121.

[45] J. Crangle, J.M. Goodman, Proc. Roy. Soc. Lond. A 321 (1971) 477-491.

Table 1

Figure 1
Click here to download high resolution image

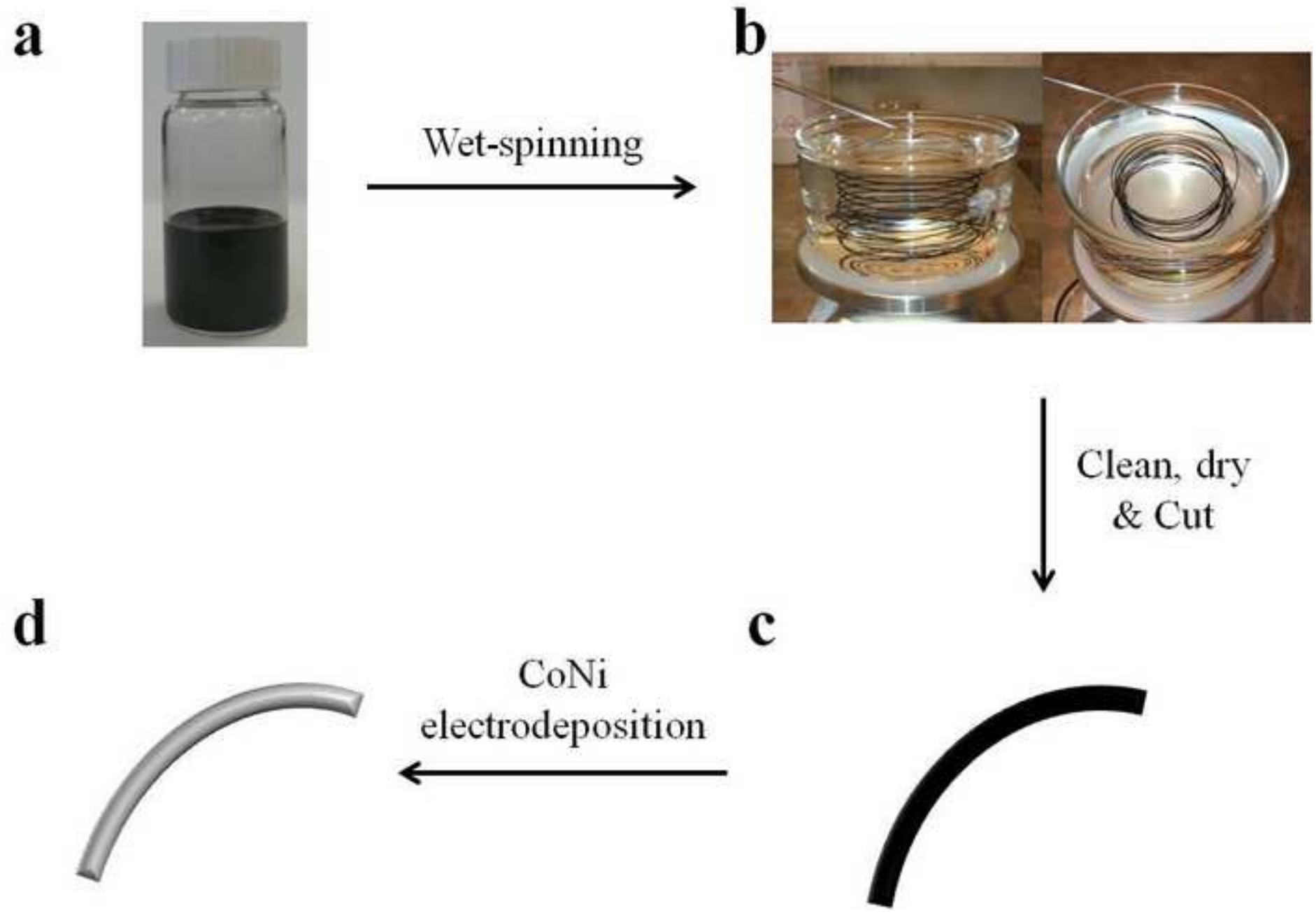

Figure 2
Click here to download high resolution image

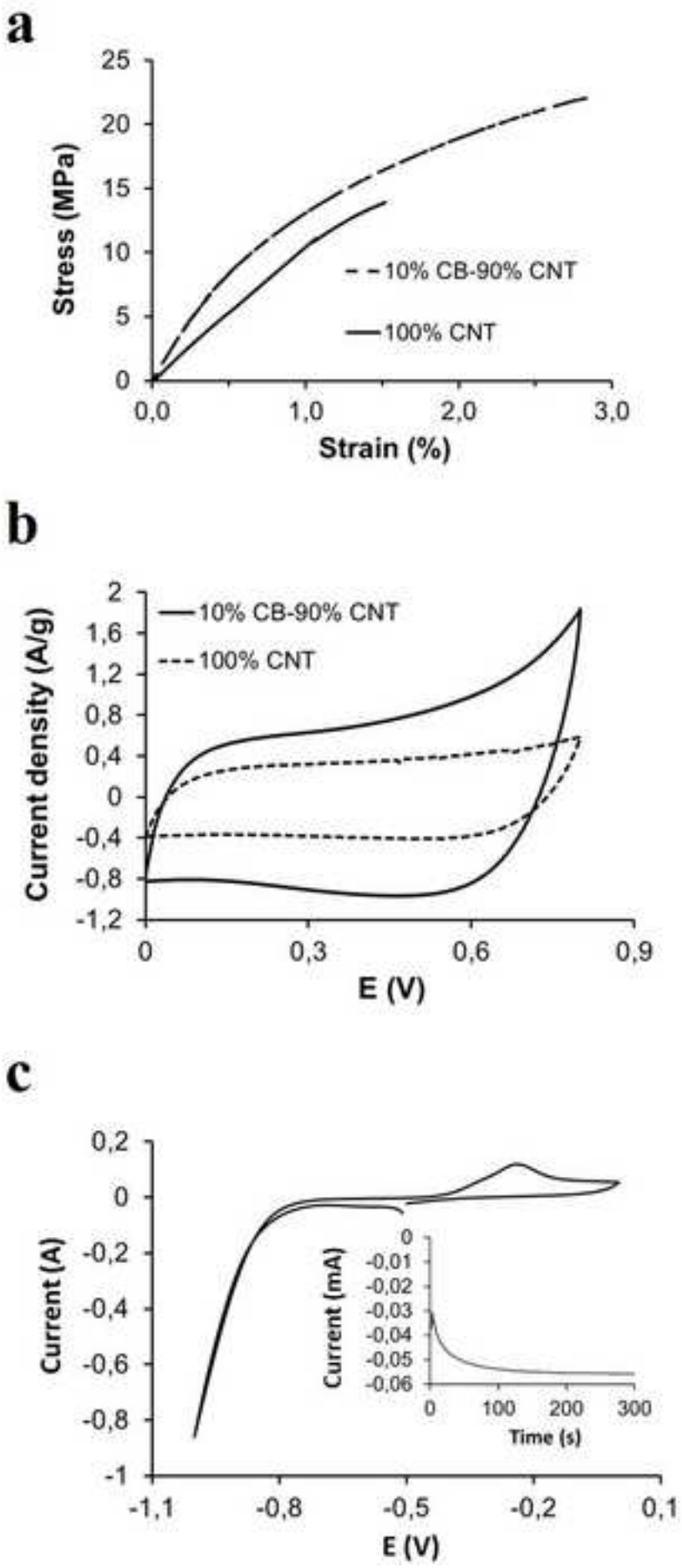

Figure 3

Click here to download high resolution image

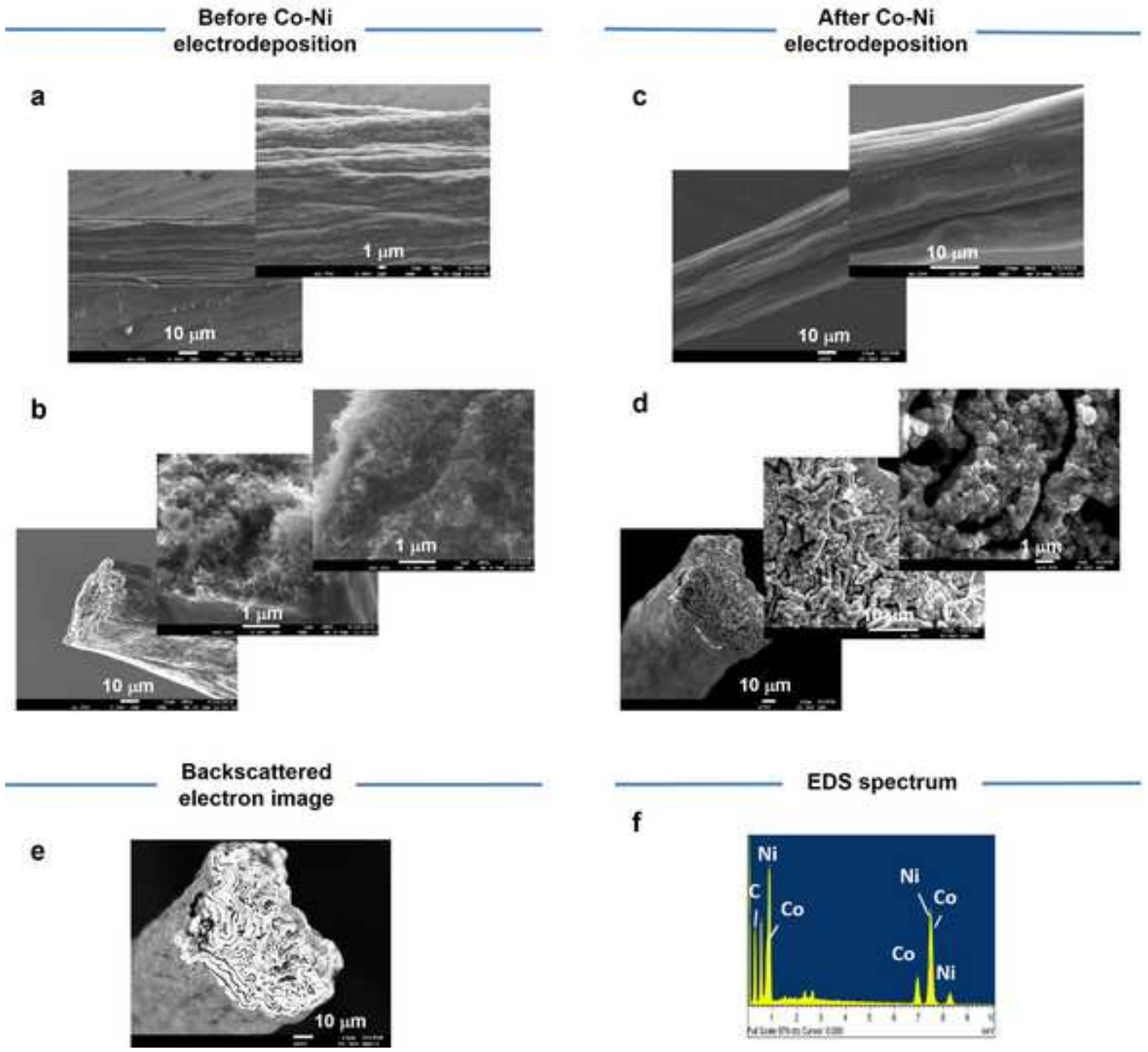

Figure 4

Click here to download high resolution image

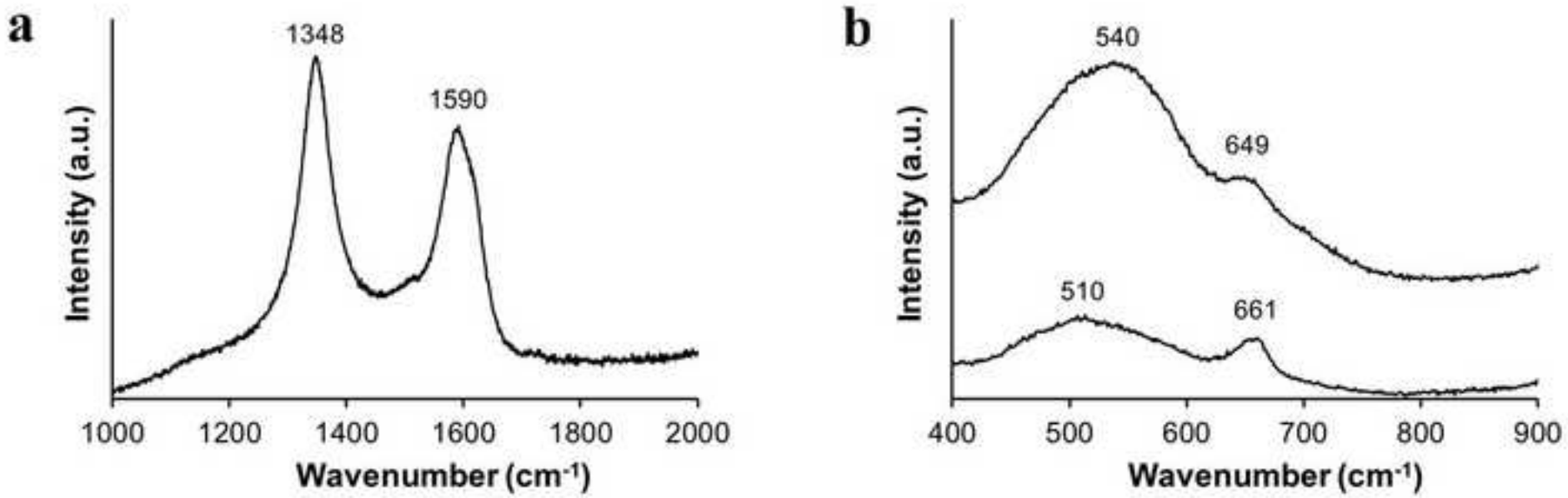

Figure 5
Click here to download high resolution image

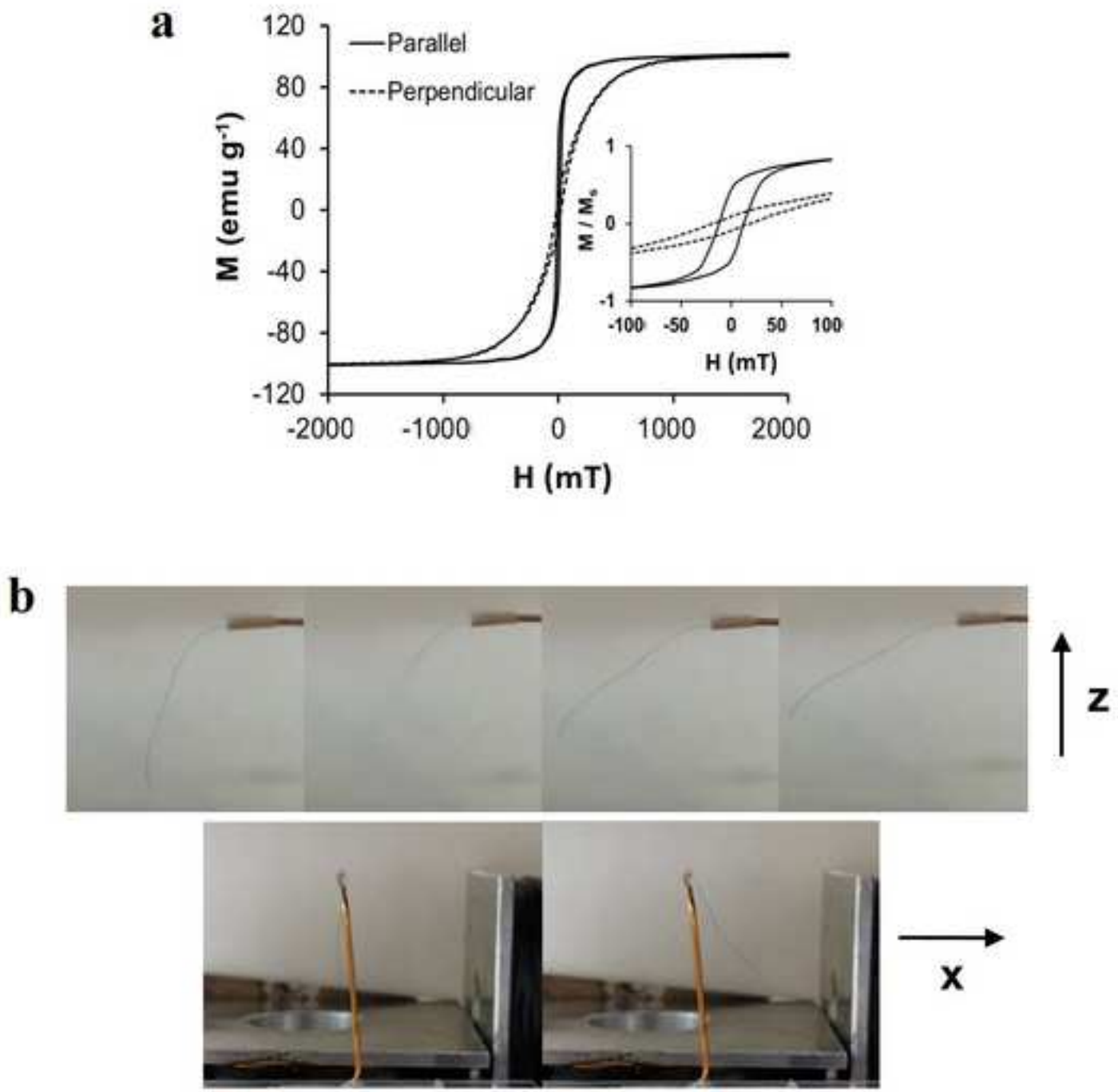

Figure 6

Click here to download high resolution image

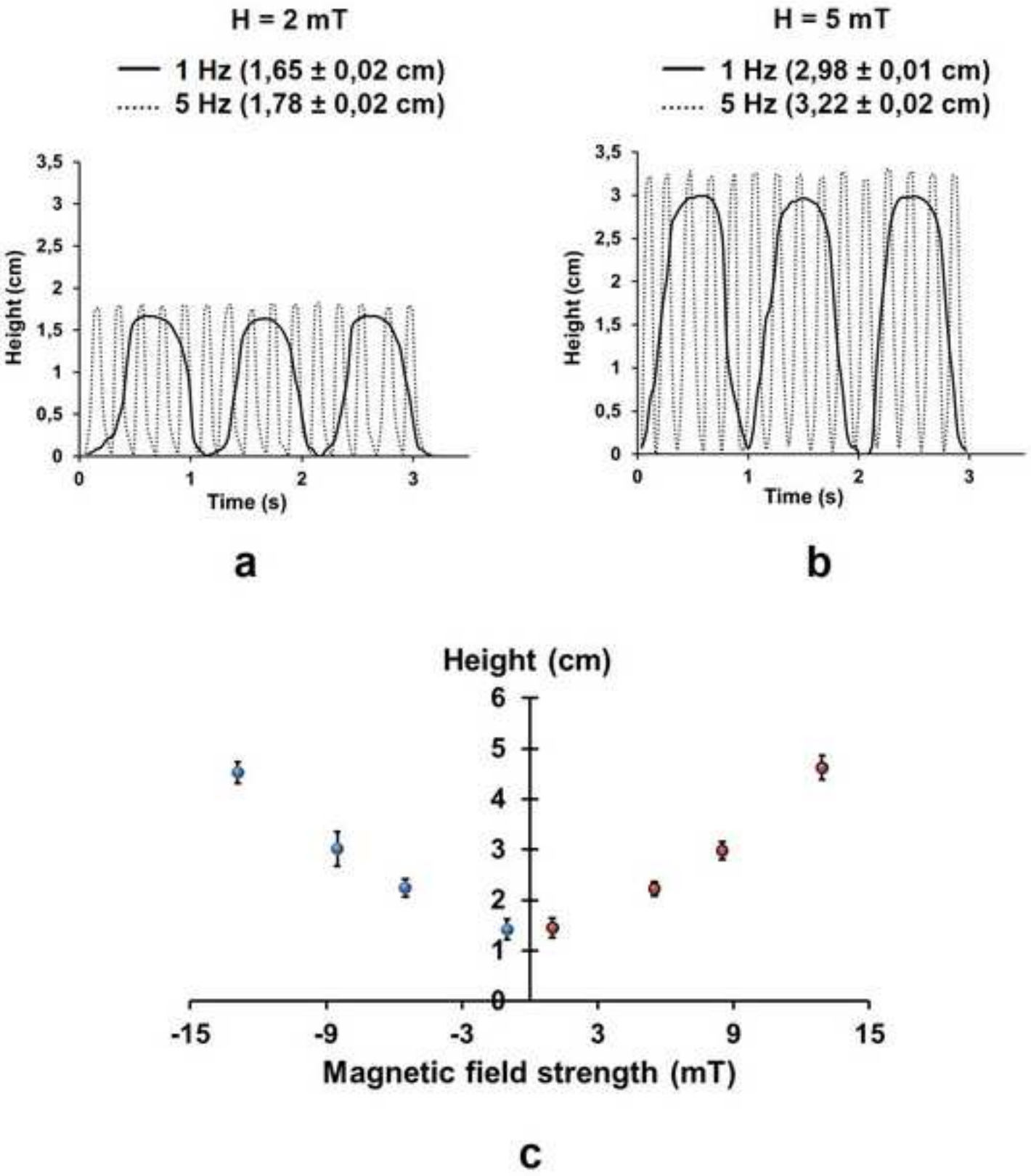

Figure 7
Click here to download high resolution image